The development of the wide-range 4D appearance function for breakage characterisation in grinding mills

P Yu[a], W Xie[b], L X Liu[c], M S Powell[a,*]

[a] *University of Queensland, Julius Kruttschnitt Mineral Research Centre, Sustainable Minerals Institute, Indooroopilly, Brisbane, QLD 4068, Australia*

[b] *Camborne School of Mines, the University of Exeter, Penryn Campus, Penryn, Cornwall, TR10 9FE, UK. Formerly: University of Queensland, Julius Kruttschnitt Mineral Research Centre*

[c] *Department of Chemical and Process Engineering, the University of Surrey, Guildford, Surrey, GU27JP, UK Formerly: University of Queensland, Julius Kruttschnitt Mineral Research Centre*

Abstract

The Appearance function, also known as breakage distribution function, is used to describe the breakage characteristics of an ore impacted with a certain energy. It is the bedrock of comminution modelling. The range of applicability of the majority of existing appearance functions is limited to coarser sizes above a few millimetres. In the previous work, a 4D (four dimensional) appearance function model was developed based on JKRBT test data, but its applicable range was not sufficiently broad at -24.4+7.3 mm. In order to develop a more versatile appearance function model that can be used for a wide range of energy levels and feed particle sizes, drop weight tests for smaller particles with sizes ranging from 425 μm to 16 mm were carried out with the Mini JK drop weight tester. Combined with data up to 63 mm from Standard JK Drop Weight Tests, the outcomes were fitted to two types of 4D appearance functions - the P80-m based 4D model and the P80-m-q based 4D model. The proposed 4D models are more accurate and scalable than existing models. Most importantly, they can be used for a wide range of conditions, with feed particle size ranging from 425 μm to 63 mm and input specific energy from 0.1 to 2.5 kWh/t in the initial test data.

Keywords: 4D appearance function; breakage distribution function; grinding, drop weight test; ore characterisation; DWT

1. Introduction

Comminution, including crushing and grinding, is an energy intensive process in the mining industry. For example, the energy used in the comminution of gold and copper ores accounts for 0.2% of global and 1.3% of Australia's electricity consumption (Ballantyne and Powell, 2014). Thus comminution circuit optimisation is of great importance in reducing the total energy cost. In order to achieve this, it is essential to characterise the breakage properties for any ore of interest so that optimisation of the comminution circuit and operational conditions through modelling can be achieved. The relationship between the product size distribution and the applied breakage energy can be quantified through ore breakage characterisation. Based on valid breakage characterisation results used in appropriate process models, comminution circuit design, modelling, and optimisation can be achieved for a particular ore.

Ore breakage characterisation involves laboratory breakage testing work that provides the establishment of an appearance function. Among the various laboratory breakage tests, single particle breakage tests are

[*] Tel: +61 7 3365 5893; Fax: +61 7 3365 5999 Email: malcolm.powell@uq.edu.au

widely used to determine the comminution characteristics of ore particles. The first single particle breakage test was the Bond Crushing Work Index Test (Bond, 1947). Subsequently, several single particle breakage tests were developed such as the Twin Pendulum Test (Narayanan, 1985; Narayanan and Whiten, 1988); the Ultrafast Load Cell test (UFLC, also called Impact Load Cell) (King and Bourgeois, 1993; Tavares and King, 2004; Weichert and Herbst, 1986); the laboratory-scale compression crushing test (Evertsson, 1999, 2000); the Short Impact Load Cell test (SILC) (Bourgeois and Banini, 2002); the JK Drop Weight Test (Napier-Munn et al., 1996); the SMC Test (Morrell, 2004) and the JK Rotary Breakage Test (JKRBT) (Shi et al., 2009).

The appearance function, also known as the breakage distribution function, is used to describe the size distribution of the breakage progeny as a function of input energy. It is an important sub-model in a generic model structure for tumbling mills (Yu et al., 2014) and some AG/SAG mill models (Leung, 1987). In this paper, the existing appearance function models that are widely used in industry were reviewed. A new 4D appearance function, which includes the effect of feed particle size and extends the particle size to the sub-millimetre range as well as the breakage at low energy inputs, was developed and validated.

2. Review of existing appearance function models

The JK t_{10} appearance function (also known as the JK breakage model (Napier-Munn et al., 1996)), the JK Mpq appearance function (also known as the JK size-dependent breakage model (Shi, 2016)), and King's t_{10} based appearance function are widely used in industry.

An important concept proposed by Narayanan and Whiten is the family of t_n curves (Narayanan and Whiten, 1988).

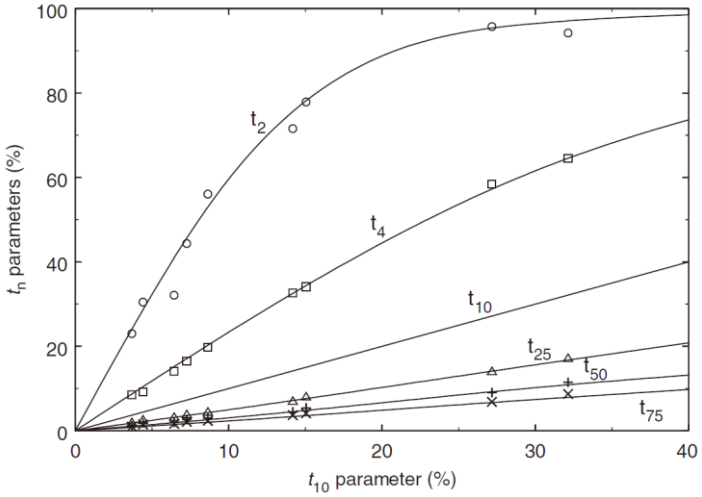

Figure 1 Relationship between t_{10} and t_ns for a copper ore. Symbols are experimental data and lines represent fitting with splines (Tavares, 2007)

In Figure 1, t_n = percentage passing an aperture of 1/n of the original ore particle size (n=2, 4, 10, 25, 50 and 75). t_{10} here is used as the reference parameter to characterise the impact breakage size distribution. For a given comminution energy, a larger t_{10} value represents a softer ore. t_{10} is also referred to as a breakage index (Napier-Munn et al., 1996).

From the above t_{10}-t_n family curves in Figure 1, if a t_{10} value is given, then all the corresponding t_n values can be determined, i.e. the complete size distribution can be obtained.

The appearance function of a certain ore is also dependent on the feed particle size and the breakage mode (Napier-Munn et al., 1996). For an AG/SAG mill, both impact breakage, and abrasion breakage occur in the mill. The drop weight tests (DWT) or rotary breakage tests (RBT) (Shi et al., 2009) can be used to measure the impact amenability of ore, generating a high-energy crushing appearance function. All the breakage test data were fitted in the form of the JK t_{10} model:

$$t_{10} = A\left(1 - e^{-b \cdot E_{cs}}\right) \tag{1}$$

where E_{cs} is the specific comminution energy (kWh/t), A and b are the ore breakage parameters determined from DWT laboratory tests, and A*b is the slope of the curve at 'zero' energy input point. It is an indicator of ore hardness. The greater the A*b value is, the softer the ore.

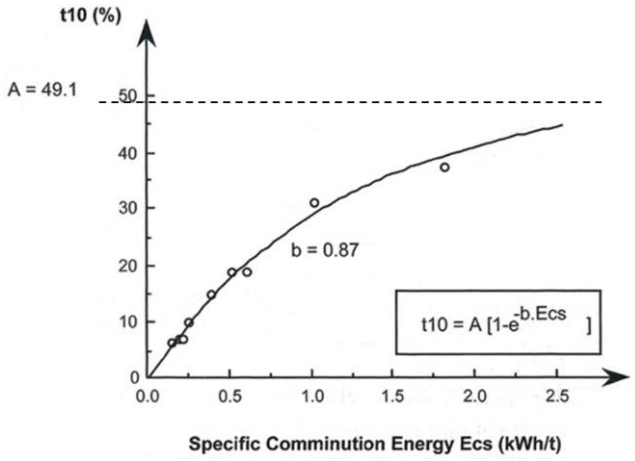

Figure 2 Effect of specific comminution energy on the breakage index t_{10} (Napier-Munn et al., 1996)

Eq. (1) is a size-averaged model, i.e., assuming that the breakage characteristics of ore are size-independent. However, Kojovic et al. (2012) found the t_{10}- Ecs relationship is size dependent (as shown in Figure 3) so the appearance function from Eq. (1) needs to be improved.

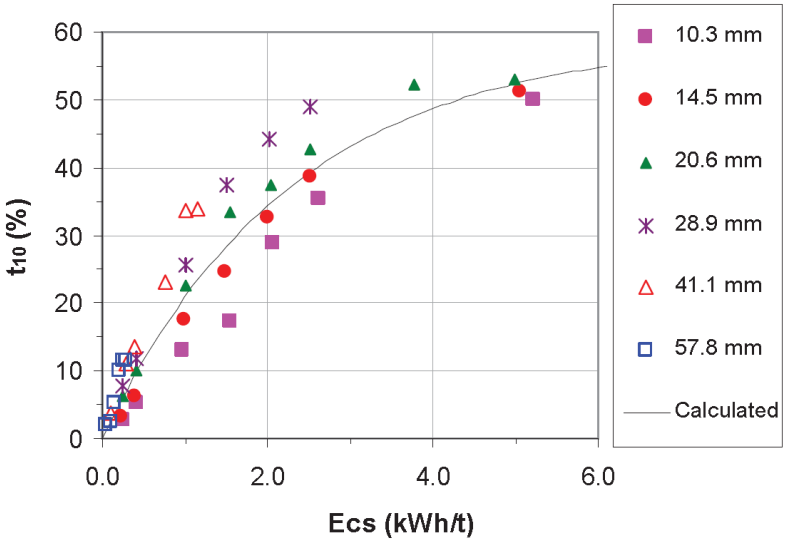

Figure 3 The deviation of t10 with one set of parameters A and b for all particle sizes (Kojovic et al., 2012)

A more recent breakage rate model for generating appearance function, the JK Mpq model was proposed to solve this problem (Kojovic et al., 2012; Shi and Kojovic, 2007; Shi et al., 2015; Shi and Xie, 2016):

$$t_{10} = M\left\{1 - e^{[-f_{mat}\cdot X\cdot k(E_{cs}-E_{min})]}\right\} \quad (2)$$

where:

M is the maximum possible value of t_{10} in impact (%);

f_{mat} is a material property (kg.J^{-1}m^{-1}) , $f_{mat} = p \cdot X^{-q}$ (Shi et al., 2015);

p and q are ore-specific constants;

X is the initial geometric mean particle size (m);

E_{cs} is the mass specific breakage energy (J.kg^{-1});

k is the successive number of impacts with the single impact energy E_{cs};

E_{min} is the threshold or minimum breakage energy (J kg^{-1}), below which the breakage will not occur. E_{min} can be ignored and set to zero for high-energy impact tests. However, for low-energy breakage tests, E_{min} cannot be set to zero (Shi, 2016).

As can be seen, the breakage appearance model, Eq. (2) takes into consideration the feed size. Thus, the JK Mpq model is a size-dependent model. It describes the product size distribution better than the JK t_{10} model, which can be taken as a size average model. (Figure 4 compared with Figure 3). The accuracy of the JK t_{10} model will worsen if the feed size range expands. The JK Mpq model can overcome a shortcoming of the JK t_{10} model by more accurately covering a wider size range than before. However, the accuracy of the JK Mpq model needs to be improved, especially when the feed size range is very wide, and this paper proposes a new method for this purpose.

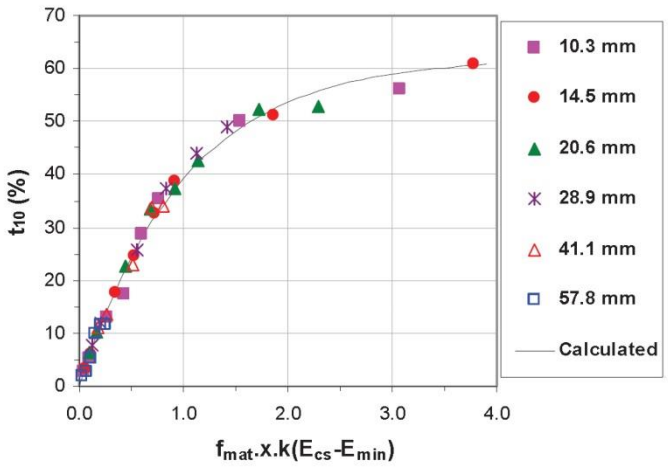

Figure 4 The updated JK model fitting result (Kojovic et al., 2012)

Both JK t_{10} and JK Mpq models need t_{10}-t_n family curves and t_{10} to calculate size distributions. Based on the truncated Rosin–Rammler distribution, King (2012) proposed an appearance function regenerated from a single value of t_{10}:

$$t_n = 1 - (1 - t_{10})^{(\frac{10-1}{n-1})^{\theta}} \quad (3)$$

where, θ is an ore-specific parameter related to ore properties, n=X/x, X is the feed size, and x is the sieve size. t_n is the cumulative percentage passing where the sieve size x is X/n. King's model is simple with only one parameter θ besides t_{10} although t_{10} may involve other parameters. However, this model is based on the

assumption that the product size distribution can be represented by the Rosin–Rammler (R-R) distribution function. Although R-R distribution is commonly used and the accuracy is acceptable in most cases, it is an empirical relationship and does not always describe the product size distribution well, especially when the specific breakage energy is low, and the feed ore size X is small. This situation is more fully discussed later in the paper.

3. Experiment using the Mini JK Drop Weight Test (mini JKDWT)

In order to develop an accurate appearance function model that cover a wide range of test conditions, single particle breakage tests at a wide range of experimental conditions were conducted. The standard JK drop weight test (standard JKDWT), which was first developed at the JKMRC in 1992 (Napier-Munn et al., 1996), was used for breakage characterisation measurement in this work. 15 sets of existing data from standard JKDWT were used for analysis. The sample size ranges are -63+53 mm, -45+37.5 mm, -31.5+26.5 mm, -22.4+19 mm, -16+13.2 mm and the specific energy (Ecs) ranges are: from 0.1 to 2.5 kWh/t. In order to develop a wider range appearance function model, this research aimed to extend the breakage sizes to much finer particle size classes, which the standard JKDWT cannot reach. The minimum drop weight of 0.1 kg for a minimum viable drop height of 10 mm provides an input energy of (0.00272/ average particle mass (g)) kWh (Eq.(4)). For particles of 5mm (assume the specific gravity SG is 4.5), for example, the minimum input energy would be 0.01 kWh/t or for a 1mm particle 1.15 kWh/t. To achieve the desired input energies, the JK mini drop weight test (mini JKDWT) was used to measure the breakage characteristics for finer-size samples from 16 mm down to 425 μm.

The Mini JK drop weight tester is a vertical drop weight impact system with an electromagnet to hold the drop weight (Figure 5). The standard ball was replaced with a steel bar so as to enable the breakage of the monolayers of particles for the small particle sizes. Table 1 shows the weight of the bars in the Mini JKDWT.

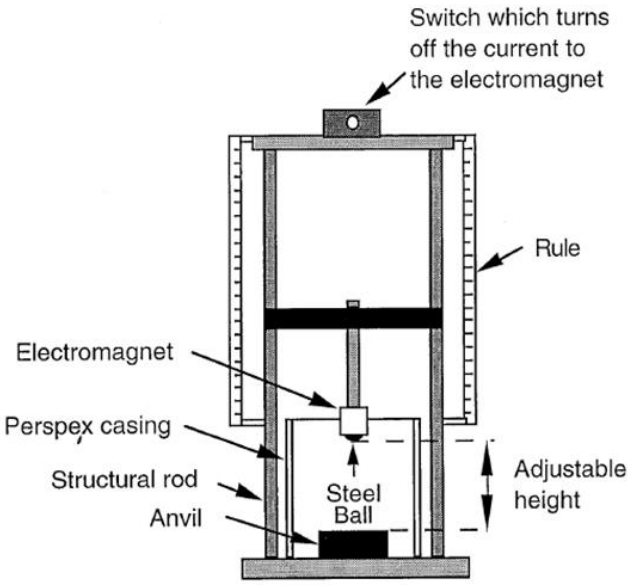

Figure 5: Schematic diagram of Mini JKDWT tester (Man, 2000)

Table 1 Drop weight bars of Mini JKDWT

Bars	Mass of Bar (g):	length (mm)	Diameter (mm)
No.1	99.64	15.8	32.0
No.2	170.52	45.3	24.9
No.3	426.93	69.1	31.9
No.4	1617.59	105.8	50.1
No.5	1901.98	124.0	49.9
No.6	2884.21	129.5	60.0

The control of required energy level for breakage is implemented based on gravitational potential energy calculation. The schematic diagram of the Mini JKDWT is shown in Figure 5 and Figure 6.

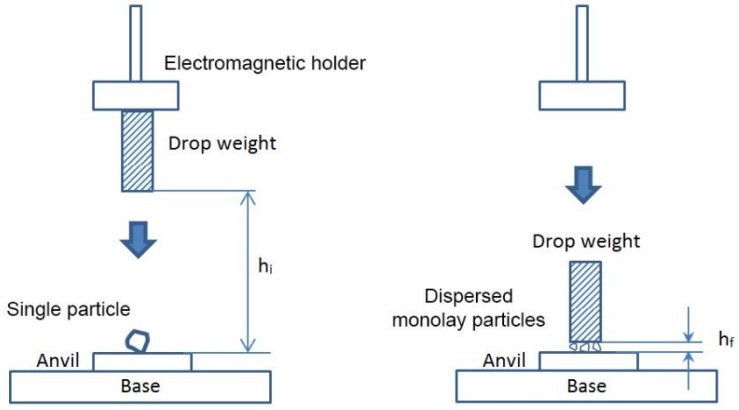

Figure 6: Schematic diagram of breakage energy calculation

The breakage energy is (Napier-Munn et al., 1996):

$$Eis = \frac{0.0272 M_d (h_i - h_f)}{\overline{m}} \quad (4)$$

where;

Eis is the input specific breakage energy (kWh/tonne),

M_d is the mass of the drop weight (kg),

h_i and h_f are the initial and final heights respectively (cm), and

$\bar{m}$ is the average particle mass (g).

With a given drop weight and the required energy level, the height of the drop weight can be predetermined. The maximum drop height difference and the maximum energy which this tester can provide are around 61 cm and $4.785*10^{-6}$ kWh. For single particle breakage of the size class -16+13.2 mm, the maximum specific energy which this tester can provide is around one kWh/tonne.

For small particles, it is impractical to use even this mini JKDWT over the desired energy ranges as the drop weight would have to be tiny. A dispersed monolayer impact method was applied to overcome this shortcoming. A dispersed monolayer of particles was used to minimise particle interaction while allowing many particles to be broken with a single impact. An air level was used to ensure the drop weight face is parallel to the anvil so as to provide an even energy input across the particles. The assumption of the

equivalence of the monolayer multiple particle breakage versus the single-particle breakage was tested, as described below.

The ore samples used in the mini JKDWT were from the Cadia gold mine in Australia, and they were the same as those used in the standard JKDWT. The samples were sized into 8 size fractions: -16+13.2 mm, -11.2+9.5 mm, -8+6.7 mm, -5.6+4.75 mm, -4+3.35 mm, -2+1.7 mm, -1+0.85 mm and -0.5+0.425 mm. The specific energy levels were: 0.1, 0.5, 1.0, 1.5, 2.0 and 2.5 kWh/t. For each size fraction, particles were broken under impact at each of the 6 energy levels, giving 45 size-energy combinations. The breakage energy was controlled by the mini JK Drop Weight Tester. For each size-energy combination, a series of breakage tests were conducted. For size fractions greater than 8 mm, single particle breakage was used for each test, and normally 30-50 particles were broken for each size-energy combination. For size fractions less than 3.35 mm, monolayer multiple particle breakage was used for each test and normally over 30 tests were conducted for each size-energy combination. For size fractions -4+3.35 mm, -5.6+4.75 mm, and -8+6.7 mm, both single particle breakage and monolayer multiple particle breakage were conducted for comparison. The detailed test plan is shown in Table 2. The size range was -16 + 0.425mm; the specific energy Ecs range was 0.1-2.5 kWh/t. In total, 3010 drops of 45 size-energy combinations were conducted. For size classes -1+0.85 mm and -0.5+0.425 mm, the number of particles per test was approximated based on the mass. For other size classes (-16+1.7 mm), the number of particles per test was counted.

Table 2 Test plan of Mini JKDWT

Ecs (kWh/t) / No.particles /test×Test times / Size (mm)	**0.1**	**0.5**	**1.0**	**1.5**	**2.0**	**2.5**
-16 +13.2 (single)	1×30	1×30	1×30	-	-	-
-11.2 +9.5 (single)	1×30	1×30	1×30	1×30	1×30	1×30
-8 +6.7 (single)	1×30	1×30	1×30	1×30	1×30	1×30
-8 +6.7 (multiple)	3×50	3×50	3×50	3×50	3×50	3×50
-5.6 +4.75 (single)	1×50	1×50	1×50	1×50	1×50	1×50
-5.6 +4.75 (multiple)	5×50	5×50	5×50	5×50	5×50	5×50
-4 +3.35 (single)	1×120	1×120	1×120	1×120	1×120	1×120
-4 +3.35 (multiple)	5×50	5×50	5×50	5×50	5×50	5×50
-2 +1.7 (multiple)	50×30	50×30	50×30	50×30	50×30	50×30
-1 +0.85 (multiple)	100×80	300×30	300×30	300×30	300×30	100×80
-0.5 +0.425 (multiple)	2000×30	2000×30	2000×30	2000×30	2000×30	2000×30

The breakage product for each size-energy combination was collected and sized to get the product size distribution.

For -2 mm particles, the dispersed monolayer multiple particle breakage method was applied (Figure 7). All the particles for one multiple-particle breakage test were placed on the anvil forming a dispersed monolayer of particles with no overlap to avoid the interaction of adjacent particles (Figure 8).

Figure 7: Dispersed monolayer multiple particle breakages for size < 2 mm

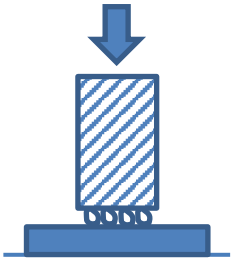

Figure 8: Schematic diagram of dispersed monolayer multiple particle breakages for size < 2 mm

Ideally, if the drop weight is parallel, the energy of the drop weight can be evenly distributed to each particle in the dispersed monolayer multiple particle breakage method if the particles have the same shape and size. However, the shapes and sizes of particles are different in reality. Consequently, energy is not evenly distributed among particles, especially at very low impact energy. It can be envisaged that some smaller particles may not be impacted by the drop weight while the particles with larger height support the drop weight. It is reasonable to believe that the error caused by uneven energy distribution is more indistinctive when the size difference is less, and the specific breakage energy is higher. To show whether there is a significant difference between single particle breakages and monolayer multiple particle breakages, the rocks at -4 +3.35 mm, -5.6 +4.75 mm, -8 +6.7 mm were tested with the above two breakage modes and the results were compared. Figure 9 shows the comparison between the two breakage modes for the size fraction -4 +3.35 mm. The multiple particle breakages resulted in slightly coarser products, but this difference is negligible for size class -4 +3.35 mm. Such comparison between single particle breakage and dispersed monolayer multiple particle breakage has also been made for the -5.6 +4.75 mm and -8 +6.7 mm size classes. The comparisons indicated an error trend: the difference between single particle breakages and multiple particle breakages diminishes as the size reduces. This is because the shape difference among coarser monolayer particles is more prominent than that in finer monolayer particles. The competent particles which are not fully broken by one impact will hold up the weight and result in the impact energy being unevenly distributed. Given that the error of -4 +3.35 mm is so small, it is believed that for sizes below 2 mm, the error is even smaller and can be neglected. Thus, the results of dispersed monolayer multiple particle breakages for -2 mm were combined with the outcomes of single particle breakage for +2 mm to derive the wide-range appearance function.

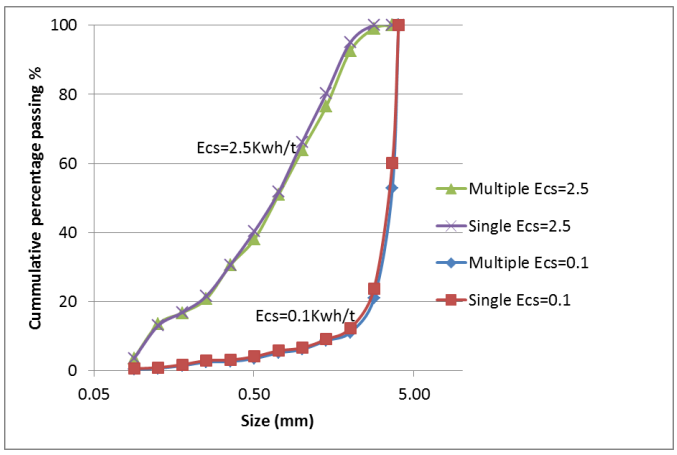

Figure 9: Comparison between the single particle breakage and the multiple particle breakage (-4.0+3.35 mm)

The procedure for Mini JKDWT was as follows:

1. Prepare the test samples with crushing or grinding
2. Choose a size-energy combination
3. For the specific size class, choose a drop weight and calculate the pre-determined height
4. Conduct a series of drop weight tests for the given size-energy combination
5. Collect all the products and size them to get product size distribution
6. Choose another size-energy combination and go to step 3 until all combinations are completed.

Some typical test results are shown in Figure 10 and Figure 11. It is apparent that with the increase of specific energy and the decrease of original rock sizes, the products become progressively finer. It is also most notable in Figure 12 that the form of the appearance function changes dramatically as the original size decreases, with steeper curve shape of product size distribution for the finer feed particles, which means a narrower size distribution.

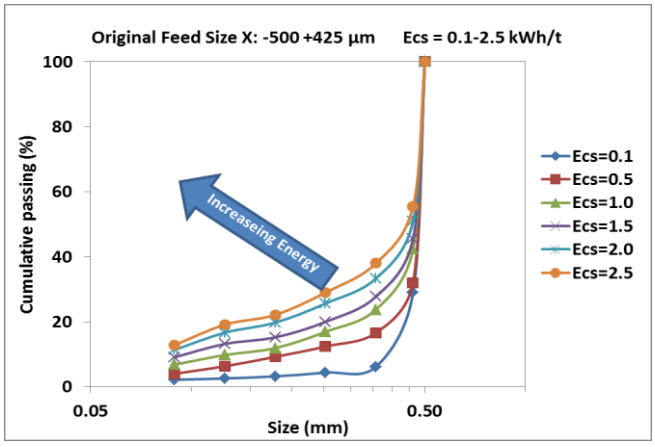

Figure 10: Product size distribution of X= -500 +425 µm at different Ecs

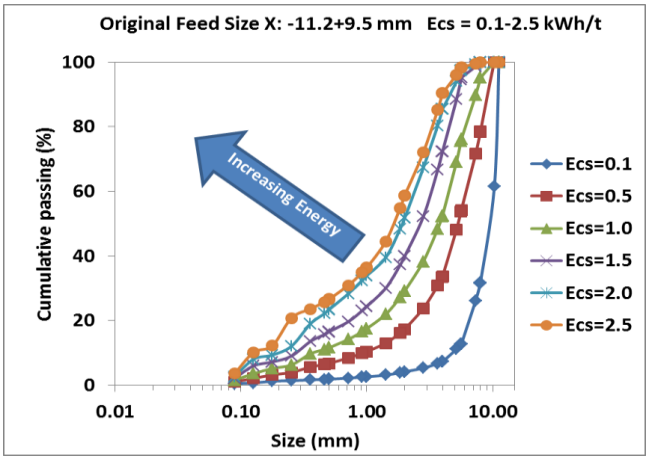

Figure 11: Product size distribution of X= -11.2 +9.5 mm at different Ecs

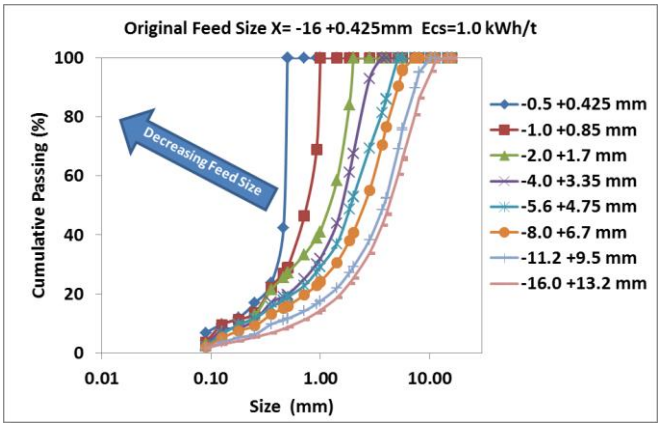

Figure 12: Product size distribution of Ecs=1.0 kWh/t at different feed size X

4. 4D-m appearance function model

45 sets of Mini JKDWT data and the existing 15 sets of standard JKDWT data were collected. There was an overlap of the two test results for X= -16+13.2 mm, Ecs=1.0 kWh/t, measured by standard JKDWT and mini JKDWT respectively and the outcome from standard JKDWT was used. Thus after eliminating overlapped data, a total of 59 sets of data were analysed to develop the 4D appearance function model.

Each set represents a product size distribution for a combination of size and energy. The product size distribution P is related to the original sizes of feed ore X (mm), ore characteristics, and input specific comminution energy Ecs (kWh/t). For a given ore, the cumulative percentage passing (P %) at a sieve size class is determined by X (mm), Ecs (kWh/t), and the sieve size class x (mm).

$$P = f_1(X, Ecs, x) \tag{5}$$

or,

$$f_2(P, X, Ecs, x) = 0 \tag{6}$$

where, f_1 and f_2 are function forms. P is a three-variable function (Eq. (5)); and in Eq. (6), there are four variables P, X, Ecs and x. Among them, X, Ecs, and x can be plotted in an X-Ecs-x 3D graph and P can be illustrated by a colour bar. Thus we obtain a virtual 4D graph which can describe product size distributions at different X, Ecs and x. Eq. (6) is named the 4D appearance function. The equation forms and parameters are derived later.

All the data from JKDWT and mini JKDWT can be shown in a virtual 4D graph (Figure 13). The fourth dimension is a colour which represents the cumulative percentage passing.

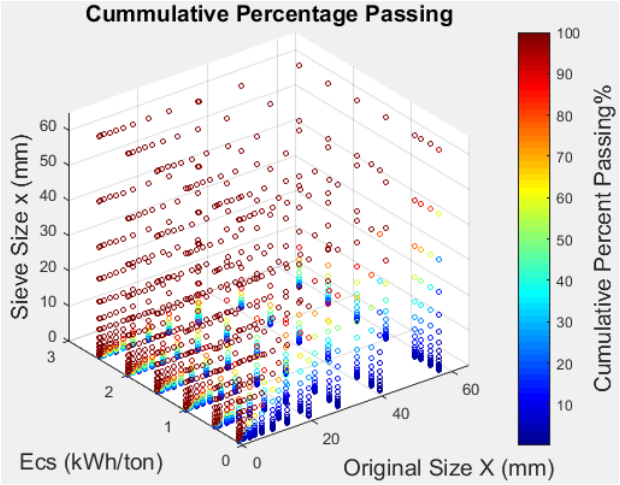

Figure 13 Experimental data from Mini JKDWT and JKDWT tests (Ore: Cadia East)

In order to obtain better fitting which not only covers the raw data but also describes the data varying trends, the raw data were interpolated before developing a 4D model, which was verified against raw data after development. By interpolating along Ecs-axis, X-axis, and x-axis, the following graphs were obtained:

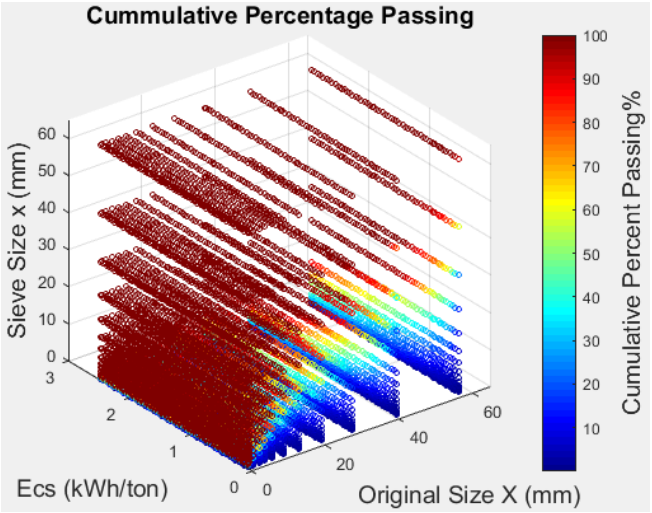

Figure 14 After interpolation with Ecs

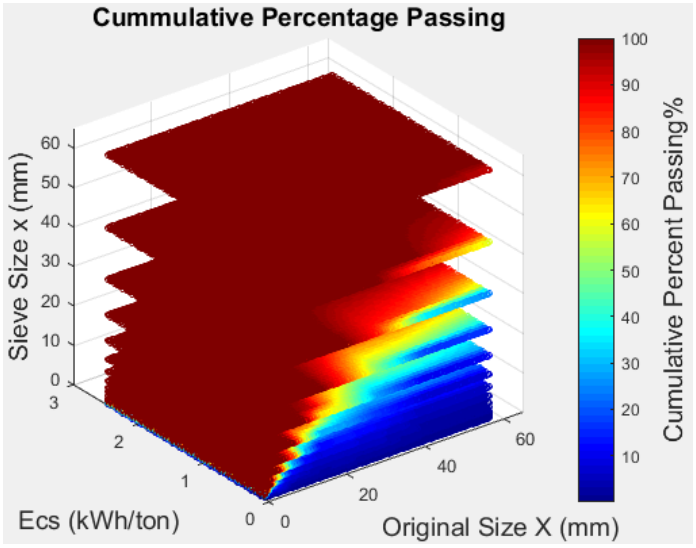

Figure 15 After further interpolation with X

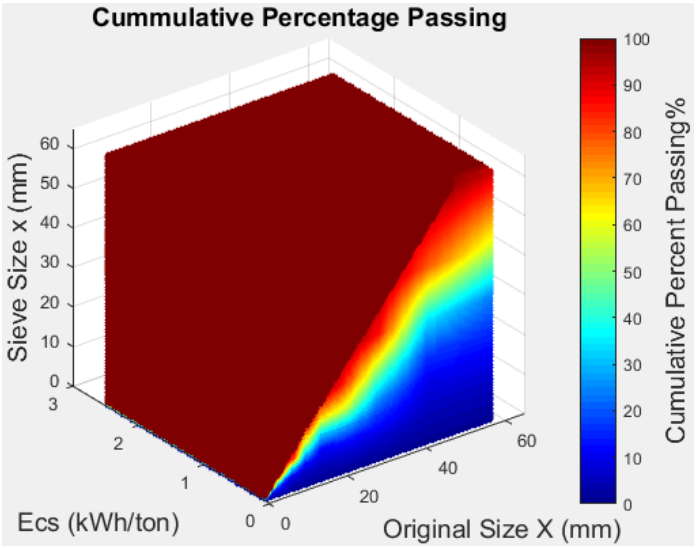

Figure 16 After the third interpolation with sieve size

In fact, the 4D graph (Figure 16) consists of a large number of columns, each representing a product size distribution for a combination of original feed ore size X and input specific energy Ecs. Generally speaking, P80-m Weibull distribution (Rosin-Rammler distribution, abbreviated as R-R) (Wills and Napier-Munn, 2006) is always used to describe the cumulative percentage passing after breakage:

$$passing = 100 * \left[1 - e^{\left(ln(0.2)\left(\frac{x}{P80}\right)^m\right)}\right] \quad (7)$$

where P80 is the size where the cumulative percentage passing is 80%, and x is the sieve size class.

There are two parameters, P80 and m in Eq.(7). In fact, both P80 and m are the two-variable functions of original feed ore size X and input specific energy Ecs:

$$P80 = f(X, Ecs) \quad (8)$$

$$m = g(X, Ecs) \quad (9)$$

The P80 values can be derived from the experimental data using reverse-interpolation method and m values can be fitted using Eq. (7) and existing experimental data. Thus for each vertical column, the parameters P80

and “m” are obtained, which represents a cumulative percentage passing curve under a breakage condition (The condition is represented by feed size X and input specific energy Ecs).

Given the known P80, m, X, Ecs, which are directly measured and calculated from experiments, the original data were plotted on 3D graphs (P80-X-Ecs and m-X-Ecs graphs) and the relationships between P80 and X-Ecs and between m and X- Ecs were analysed. Exponential functions and polynomial functions were used in a trial and error method to fit the model. The detailed forms of Eq. (8) and (9) are fitted:

$$P80 = \{e^{[(10X_{nd}^3+\alpha X_{nd}^2+\beta X_{nd}+1)e^{\gamma Ecs_{nd}^{\delta}}]}\} - 1 \qquad (10)$$

where, α, β, γ, and δ are parameters,

X_{nd} is the dimensionless feed size $X_{nd}=X/X_{top}$,

Ecs_{nd} is the dimensionless specific energy $Ecs_{nd}=Ecs/Ecs_{top}$,

X is the original size of feed ore (mm),

X_{top} is the top feed ore size (mm),

Ecs is the specific energy (kWh/t), and

Ecs_{top} is the top specific energy (kWh/t), the largest Ecs value among all the Ecs values at different X.

The dimensionless forms of the feed size and the specific energy make the model more scalable.

$$m = e^{\left[\frac{\lambda X_{nd}^{\eta} Ecs_{nd}^{\kappa}}{1+\phi X_{nd}^{0.02}+\psi Ecs_{nd}^{0.1}} - 5\right]} \qquad (11)$$

where λ, η, κ, ϕ, ψ are fitting parameters.

Thus we have developed two groups of parameters: one group (α, β, γ, and δ) for P80 and the other group (λ, η, κ, ϕ, ψ) for “m”. Table 3 shows the ore-specific fitting parameters in Eq.(10) and Eq.(11):

Table 3 Parameters in the 4D-m model

P80 parameters	α	β	γ	δ	
Value	-19.1586	12.7187	-0.6888	0.7504	
m Parameters	λ	η	κ	ϕ	ψ
Value	0.6142	-0.1085	-0.1344	-0.7338	-0.1435

After transposition and taking the logarithm of both sides of Eq. (10) and Eq.(11), the relationships between P80, m and X, Ecs were presented in the surface plots in Figure 17 and Figure 18 together with the original data points. The colour bar in Figure 17 represents the value of Ln(P80+1) and that in Figure 18 indicates the value of Ln(m) +5.

P80 size is often used as a measurement for product size in the industry. A smaller value of P80 indicates a finer product size. “m” determines the shape of the product size distribution. A larger “m” indicates a steeper product size distribution curve. When the original feed ore size X increases and the specific energy Ecs decreases, P80 will increase, which means coarser products were measured (Figure 17). When the original feed ore size X decreases and the specific energy Ecs decreases, “m” value will increase, indicating that the steeper product size distribution curves and a narrower range of product sizes were measured.

When the dimensionless feed size X_{nd} ($X_{nd}=X/X_{top}$) is less than 0.0345 (in this case, the top geometric mean feed ore size X_{top} is 57.78 mm, so the original feed size X is below 2 mm), the "m" value was large, implying a steep product size distribution curve (Figure 18) and a narrow range of product sizes.

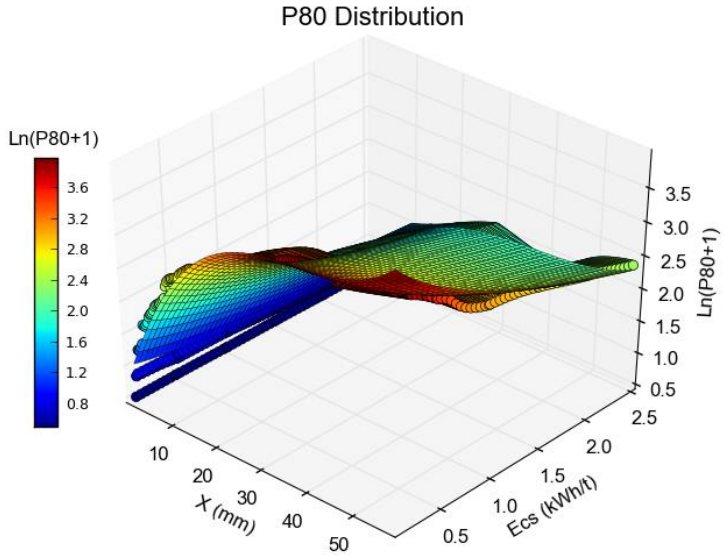

Figure 17 P80 varying with Ecs and X

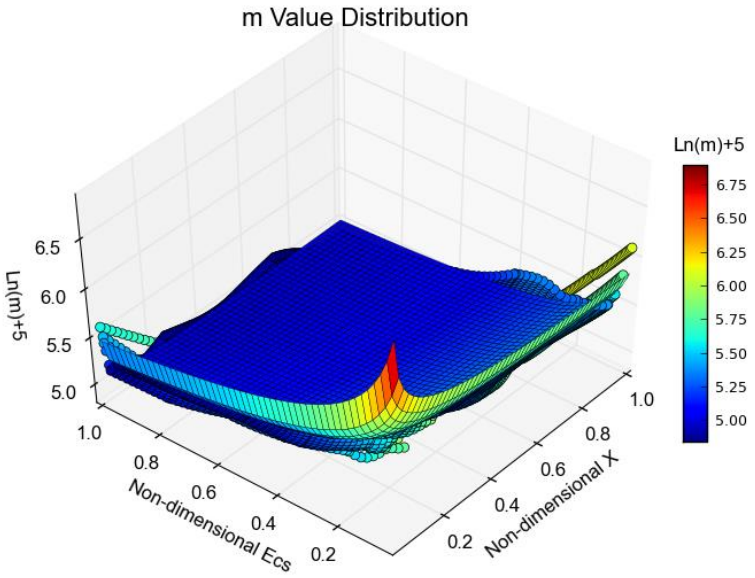

Figure 18 Parameter m varying with Ecs and X

Eqs (7), (10) and (11) constitute a 4D appearance function model for a given ore (Cadia in this case). It is named the 4D-m appearance function model because it is based on the P80-m Weibull distribution. For any given feed ore size X and input specific energy Ecs, P80 and "m" can be calculated with Eqs (10) and (11). Submitting P80 and "m" into Eq. (7), the cumulative percentage passing can be predicted. This 4D model was developed through fitting with test data and was validated against those test data to see the fitting accuracy. As long as the model accuracy is confirmed, it can be used to predict the energy-size characterisation of that specific ore in future.

5. 4D-mq appearance function model

The P80-m Weibull distribution (Rosin-Rammler distribution) is widely used in industry to describe comminution product size distribution, especially where the product size distribution curve is not so steep. However, when the feed ore size X is smaller, and the specific energy is lower (e.g. X: -2 mm, Ecs: -0.5 kWh/t), the shape of the product size distribution curve is steeper and even behave like a step in a size range (e.g. Figure 12). The P80-m Rosin-Rammler distribution cannot describe the steep curves well, and especially at smaller sieve sizes with larger errors. In order to solve this problem, the amended form of Rosin-Rammler P80-m distribution was introduced:

$$passing = 100 * \left[1 - 0.2e^{q(1-(\frac{x}{P80})^m)}\right] \quad (12)$$

where q is an ore-specific constant around $ln(5)$ (q here is different from that in Eq.(2)). Considering the amended R-R P80-m-q distribution Eq. (12), when $q = ln(5) \approx 1.609$, Eq.(12) can be rewritten as:

$$passing = 100 * \left[1 - e^{\left(ln(0.2)+ln(5)-ln(5)(\frac{x}{P80})^m\right)}\right] \quad (13)$$

Because $ln(0.2) + ln(5) = 0$, Eq. (13) or Eq.(12) is equivalent to the traditional R-R distribution Eq.(7). When the sieve size x tends to zero, the cumulative percentage passing from traditional R-R distribution Eq.(7) is zero, which is theoretically correct. However, the limit of cumulative percentage passing from the amended R-R distribution Eq. (12) is not zero when x approaches zero. Fortunately, the industry is not so concerned with the cumulative percentage passing at extreme small progeny sizes (e.g. < 1 μm) in most cases. For example, the most common minimum sieve mesh size in several standardised mesh series is 25 μm and can reach down 5 μm (for particles below 5 μm, laser diffraction sizing technique is preferable). Even in ultrafine grinding (UFG), the progeny sizes are around several microns which are far greater than zero limit. Thus the proposed amended R-R relationship Eq. (12) can be used to describe breakage characteristics. In this case, the smallest bottom sieve size is 0.075 mm, which is far more than zero mm (the limit of sieve size), so the amended R-R distribution Eq. (12) can be used to develop the P80-m-q based 4D model.

In a 4D graph, each column represents a product size distribution under a combination of X and Ecs. This distribution can be described with P80-m-q relationship Eq. (12). Thus each column has a corresponding set of P80, m, and q. q is linked to P80 and m. As long as P80 and m are determined, q can be determined. According to empirical observations, q value can be determined by the following q value determination map (Figure 19). Check the P80 and m values to determine which area should be applied and then q value can be found in Table 4.

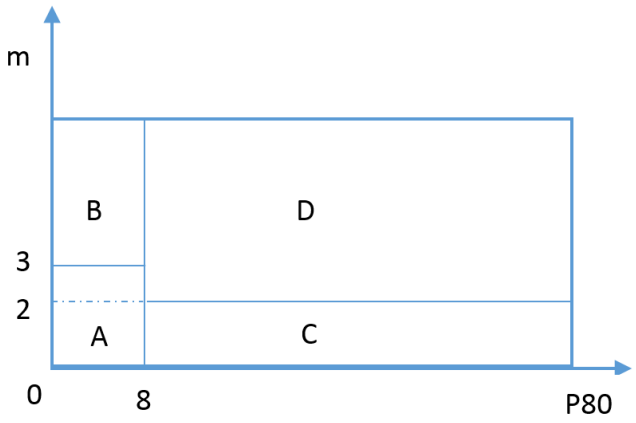

Figure 19 Determination of q values in P80-m plot

Table 4 q values in different areas of P80-m plot

Area in P80-m plot	A	B	C	D
Empirical Observation for "q"	1.55	1.57	1.58	1.6

Eqs (12), (10) and (11) constitute the other 4D appearance function model for a given ore (Cadia in this case). It is named the 4D-mq model because it is based on the P80-m-q distribution relationship (Eq.(12)). For any given feed ore size X and input specific energy Ecs, P80 and "m" can be calculated with Eqs (10) and (11). The parameters for 4D-mq model are:

Table 5 Parameters in the 4D-mq model

P80 parameters	α	β	γ	δ	
Value	-19.1586	12.7187	-0.6888	0.7504	
m Parameters	λ	η	κ	ϕ	ψ
Value	0.5716	-0.1201	-0.1268	-0.7654	-0.1230

"q" can be determined from Figure 19. Given P80, "m" and "q", cumulative percentages passing can be predicted with Eq. (12). When the 4D-mq model is applied to different ores, the parameters should change according to breakage test data whereas the equation forms Eqs (12), (10) and (11) are unchanged. This feature makes the wide-range 4D-m and 4D-mq models more generic in nature. Of course, "q" determining map, resulted from empirical observation of the test data, should be a little bit different from ore to ore.

It is proved in the next sections that 4D-mq model can provide a better description of product size distribution overall compared with 4D-m model, especially when the product size distribution curve is very steep (e.g. at smaller sieve sizes and lower specific energy).

6. Result comparison and discussion

6.1. Other t_{10} based appearance functions

In order to compare the results of the 4D appearance function models and traditional t_{10} based model, three t_{10} based appearance functions discussed in Section 2 were applied here: JK t_{10} (Napier-Munn et al., 1996), JK Mpq models (Kojovic et al., 2012; Shi and Kojovic, 2007) and King t_{10} based appearance function (King, 2012).

Based on 59 sets of experimental raw data, a series of t_n-t_{10} family curves (Figure 20) and a table of basic appearance function data (Table 6) were obtained through interpolation.

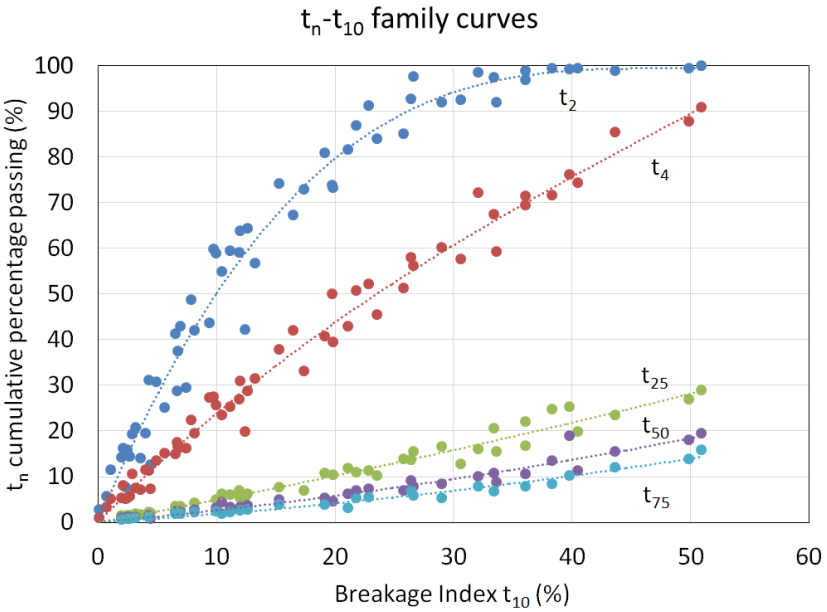

Figure 20 t_n vs degree of breakage t_{10} family curves

Table 6 Basic data for JK t_{10} appearance function

t_{10}	t_{75}	t_{50}	t_{25}	t_4	t_2
0	0	0	0	0	0
10	1.83	2.63	4.92	23.86	50.11
20	4.14	5.79	10.20	43.77	79.67
30	6.94	9.48	15.84	60.70	94.13
40	10.22	13.68	21.83	75.61	98.91
50	13.98	18.42	28.17	89.48	99.45

With the above data, if t_{10} is known, all the t_ns can be estimated through interpolation. For JK t_{10} model, t_{10} is a one-variable function of Ecs. For JK Mpq model, t_{10} is a two-variable function of X and Ecs (see Eq. (2)). Based on the experimental data, the parameters in Eq.(1) and Eq. (2) (i.e. A, b, M, p and q) can be derived (Figure 21, Figure 22, Table 7).

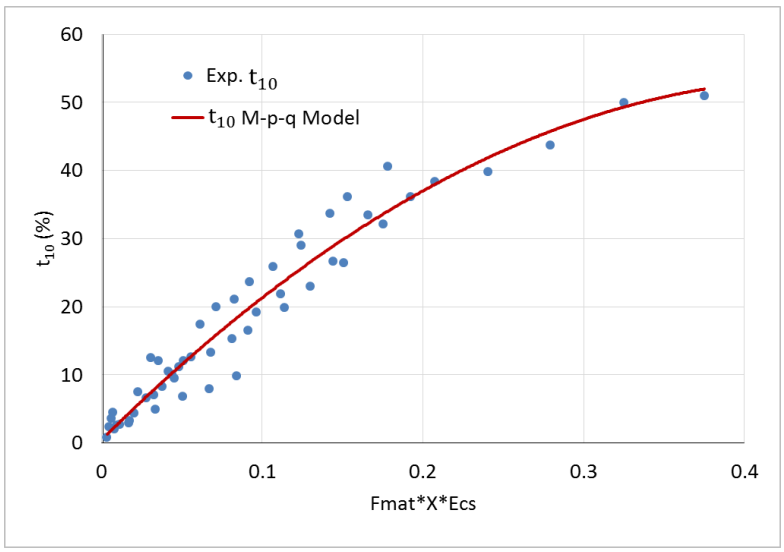

Figure 21 t_{10} vs (Fmat *X*Ecs) in the JK Mpq model

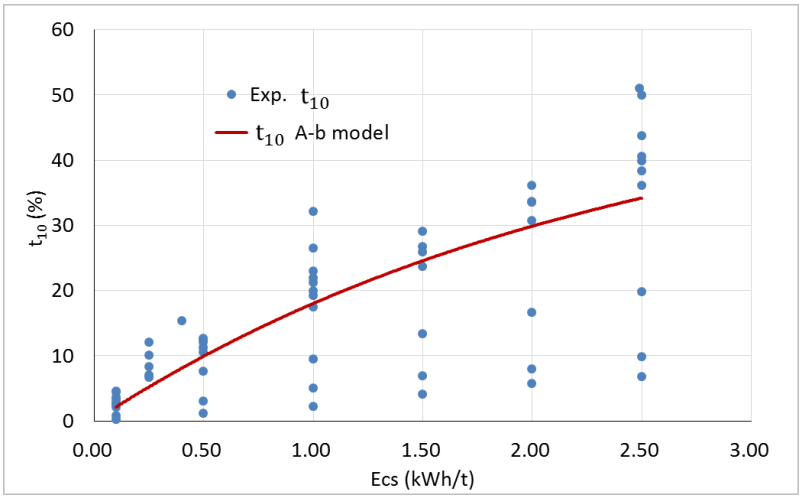

Figure 22 t_{10} vs Ecs in the JK t_{10} model

Table 7 Parameters fitted for the JK t_{10} and Mpq models

A	b	M	P	q
52.77	0.42	71.306	0.035	0.565

With the A-b relationship Eq. (1), the M-p-q relationship Eq.(2), and Table 7, given any X and Ecs combination, t_{10} can be obtained. With the basic data of t_n- t_{10} family curves, t_n can be calculated based on interpolation methods and then the product size distribution can be obtained.

King's t_{10} based model was also used to calculate production size distribution in this case. The cumulative percentage passing can be calculated with Eq.(3). The ore-specific parameter θ is 0.8 in this case, and t_{10} can be calculated with Eq. (2).

6.2. Comparison between the 4D models and the t_{10}-based models

The product size distributions from the 4D appearance function model and the three t_{10} based appearance functions were compared with the experimental data. The total 59 sets of experimental data each have an independent relationship between feed ore size and input specific energy. At each combination of feed ore size X and input specific energy Ecs, a series of sieves (bottom sieve size: 0.075 mm-53 mm, 20 size classes in total) was used to obtain the progeny size distributions. At each sieve size class, there is a cumulative percentage passing a specific combination of X and Ecs. Theoretically, there should be 1180 points. However, for larger feed sizes, some small sieve size classes were not used in experiments (e.g. bottom sieve size: 0.075-0.212 mm). Thus, the 59 sets of test data have 1135 points. In order to make the evaluation statistically correct, the standard error (SE) was used to compare performance of the models (Napier-Munn, 2014) in Eq.(14).

$$SE = \sqrt{\frac{\sum_{i=1}^{n}(passing_{(pre)} - passing_{(exp)})^2}{n-k}} \tag{14}$$

where, SE is the standard error, n is the number of points, k is the number of fitting parameters, $passing_{(pre)}$ and $passing_{(exp)}$ are respectively the predicted passing and the experimental passing. The calculation results are compared in Table 8 and Figure 23:

Table 8 Prediction accuracy comparison between the 4D and t_{10} based models

Model Type	Standard Error %
JK t_{10} model	14.9
JK Mpq model	9.8
King's t_{10} model	5.9
4D-m model	3.9
4D-mq model	3.5

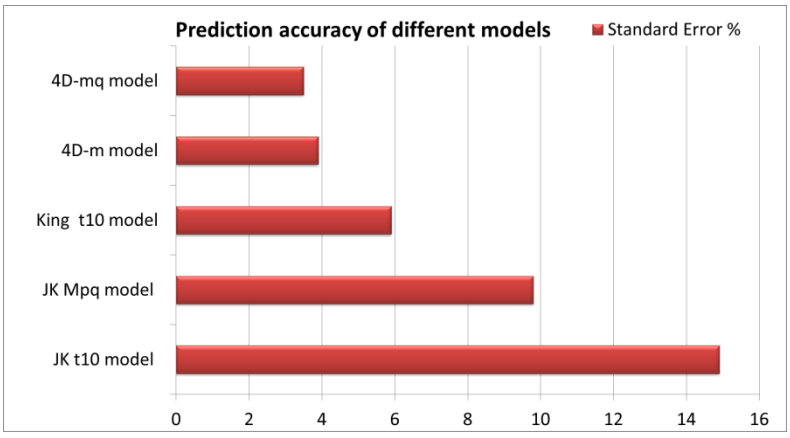

Figure 23 Comparison between the 4D appearance function model and t_{10} based models

It is apparent that the 4D models have better prediction accuracy than t_{10} based models. The JK t_{10} model has the largest inaccuracy because it is a size average model and cannot predict wide-size-range breakage. Compared with the JK t_{10} model, the JK Mpq model significantly improves the accuracy by considering feed ore size effect in breakage. However, because the JK Mpq model uses the uniform t_{10}-t_n family curves for each combination of X and Ecs (feed size and specific energy) regardless of how small the values of X and Ecs, it has a larger error than King's t_{10} based model. In fact, the shape of product size distribution curves for smaller X and lower Ecs is steeper, which cannot be well described by the JK Mpq model. In contrast, based on the truncated Rosin–Rammler distribution, King's t_{10} based model achieves a good accuracy (SE =5.9%). The 4D-mq model has the best prediction (SE =3.5%).

6.3. Validation of the 4D models against experimental data

The comparison between the experimental data and the 4D models are presented in Figure 24.

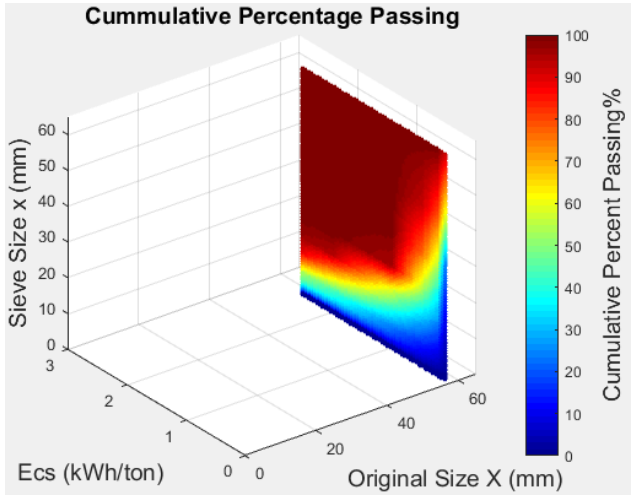
Cummulative Percentage Passing
Sieve Size x (mm)
Ecs (kWh/ton)
Original Size X (mm)
Cumulative Percent Passing%

a)

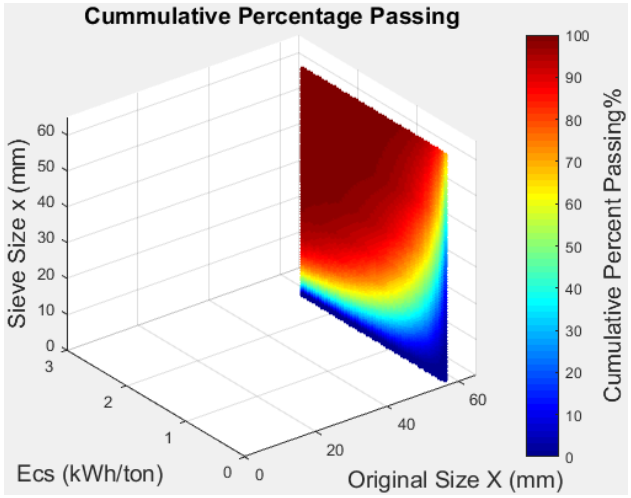
Cummulative Percentage Passing
Sieve Size x (mm)
Ecs (kWh/ton)
Original Size X (mm)
Cumulative Percent Passing%

a1)

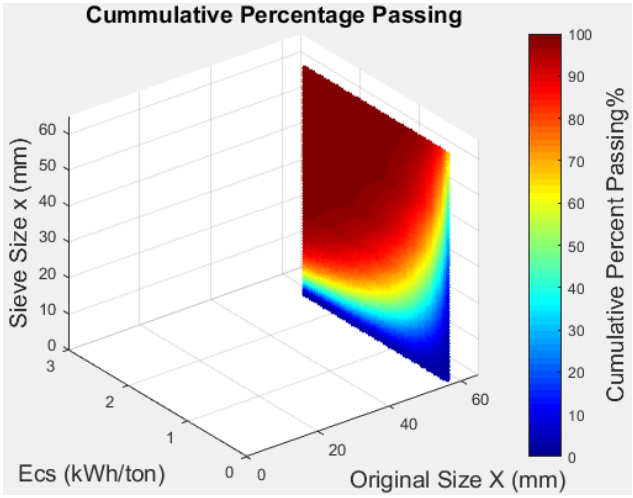
Cummulative Percentage Passing
Sieve Size x (mm)
Ecs (kWh/ton)
Original Size X (mm)
Cumulative Percent Passing%

a2)

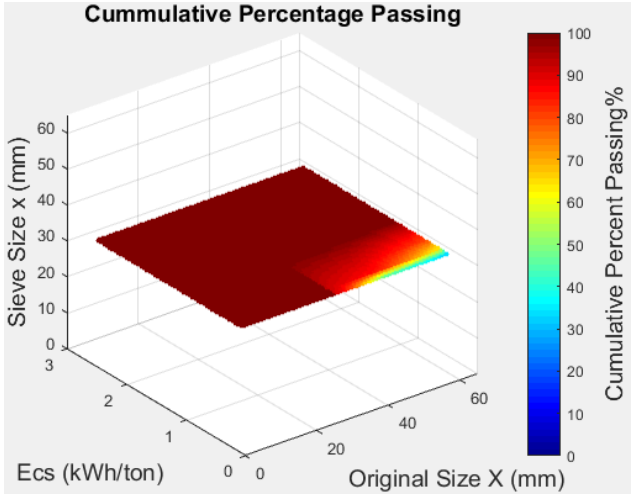
Cummulative Percentage Passing
Sieve Size x (mm)
Ecs (kWh/ton)
Original Size X (mm)
Cumulative Percent Passing%

b)

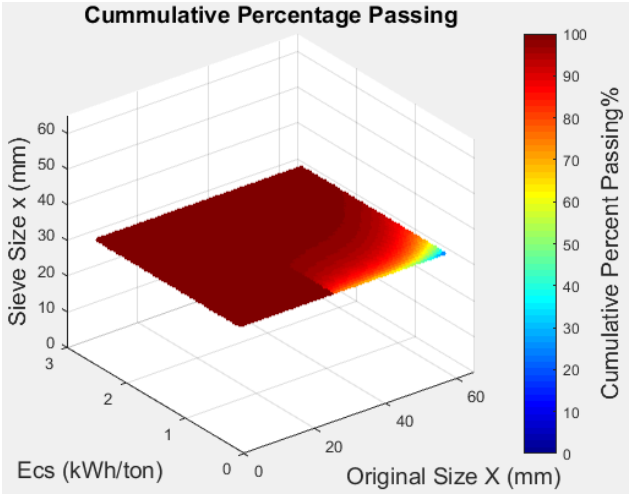
Cummulative Percentage Passing
Sieve Size x (mm)
Ecs (kWh/ton)
Original Size X (mm)
Cumulative Percent Passing%

b1)

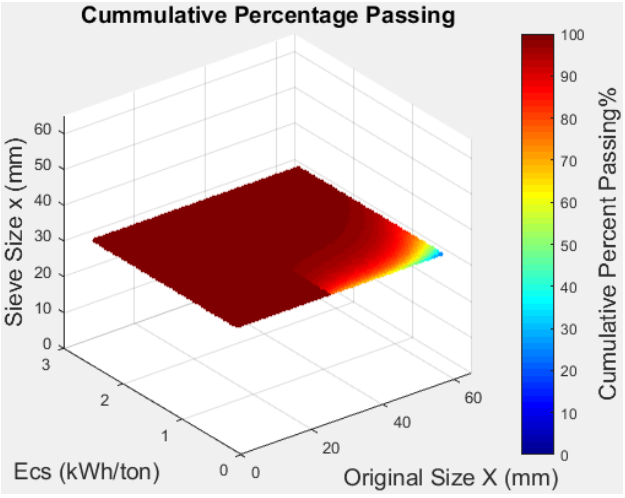
Cummulative Percentage Passing
Sieve Size x (mm)
Ecs (kWh/ton)
Original Size X (mm)
Cumulative Percent Passing%

b2)

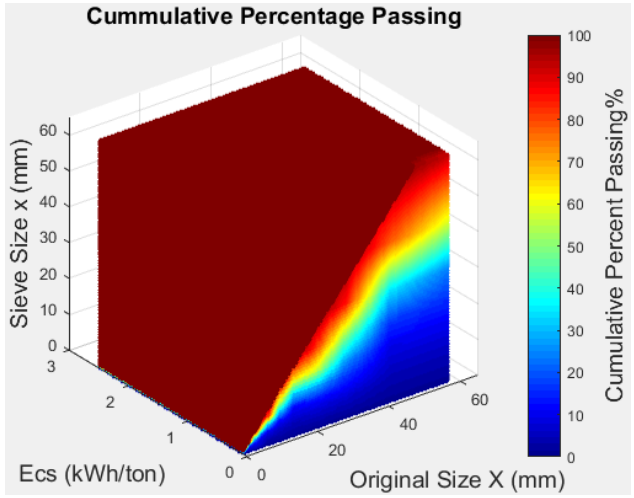

c)

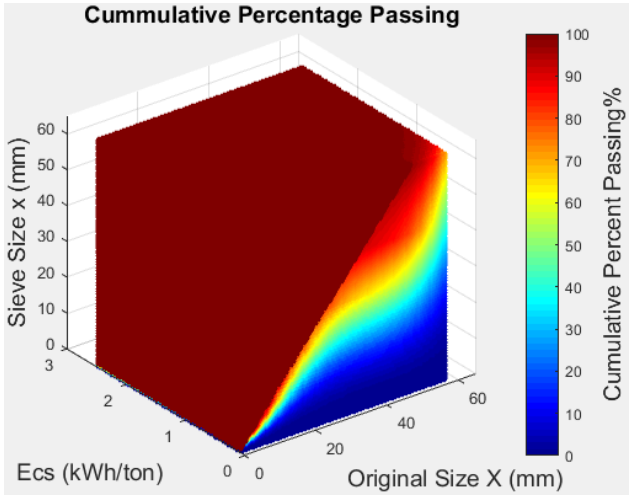

c1)

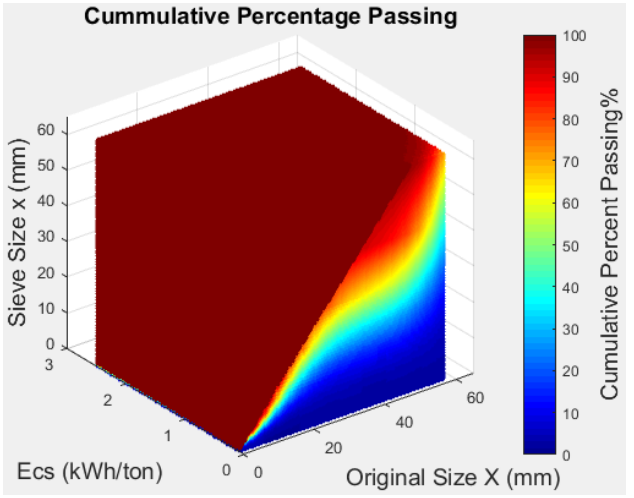

c2)

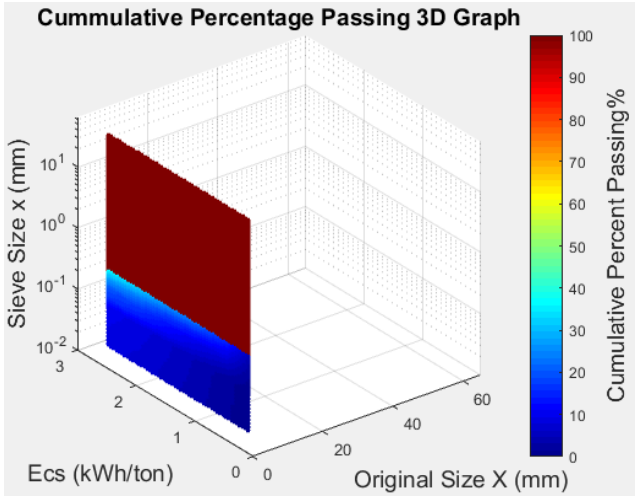

d)

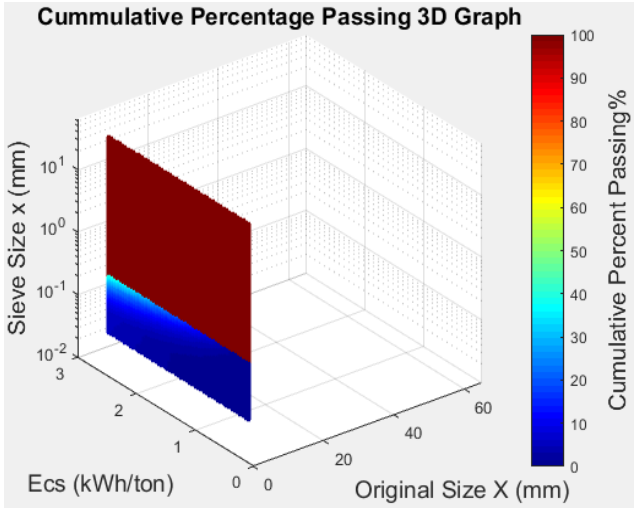

d1)

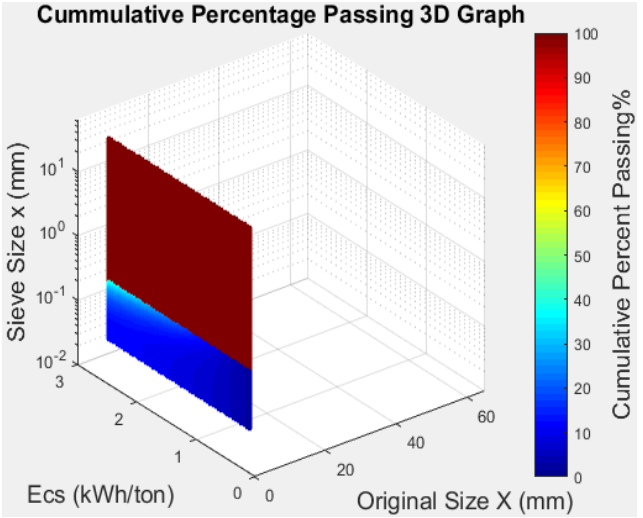

d2)

Figure 24 Comparison between Experimental data, the 4D-m model and the 4D-mq model (where, a), b), c), d): original data; a1), b1), c1), d1): 4D-m model; a2), b2), c2), d2): 4D-mq model)

Except for Figure 24 c), c1) and c2), all the graphs are sectional views of the virtual 4D cube. The X-axis is the feed size, Ecs is the specific energy, and the x-axis is sieve size. The cumulative percentage passing is expressed by colour. Figures d), d1) and d2) are plotted in X-Ecs-ln(x) semi-logarithmic coordinate to show the details in smaller sieve sizes. It can be seen that across all sectional views the predictions of the 4D appearance function models are very close to the experimental data. The 4D-m model and the 4D-mq model are very similar. However, a slight difference can be found after scrutinising the graphs. Figure d2) is more similar to Figure d) compared with Figure d1), indicating that the 4D-mq model has better prediction performance than the 4D-m model in the range of smaller sieve sizes.

Generally speaking, both the 4D-m model and 4D-mq model can predict the experimental data well. However, the 4D-m model underestimates the cumulative percentages passing at smaller sieve sizes (e.g. x < 0.212 mm), especially at smaller feed sizes (e.g. X < 2 mm) and lower energy (e.g. Ecs < 0.5 kWh/t) (Figure 25). For high energy and larger feed sizes, this underestimation is not an issue (Figure 26). This is caused by the exponential function nature of the P80-m R-R relationship. As the sieve size x approaches zero, the exponential function sharply decreases to zero. For lower energy and smaller feed sizes, the product size distribution curves are steeper, where the accelerated decrease effect is more prominent, resulting in underestimation in cumulative percentages passing. For sieve sizes below 0.212 mm, the underestimation magnitude is about 2% for the 4D-m model.

The 4D-mq model was proposed to reduce the error of the 4D-m model in the range of low energy and smaller feed sizes. It can significantly lift the curved end of the 4D-m model (Figure 25), satisfactorily predicting the cumulative percentage passing at smaller sieve sizes (x) under any combinations of feed size (X) and specific energy (Ecs). At coarser sieve sizes, larger feed sizes and high specific energy, the 4D-mq model also has a similar performance to the 4D-m model (Figure 26). Thus the 4D-mq model can replace the 4D-m model in ore breakage characterisation.

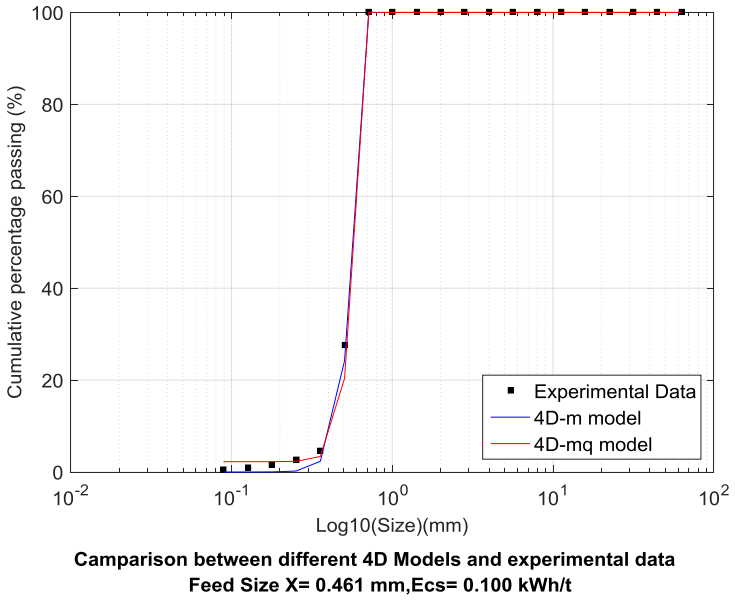

Figure 25 Size distribution comparison (X=0.461 mm, Ecs=0.1 kWh/t)

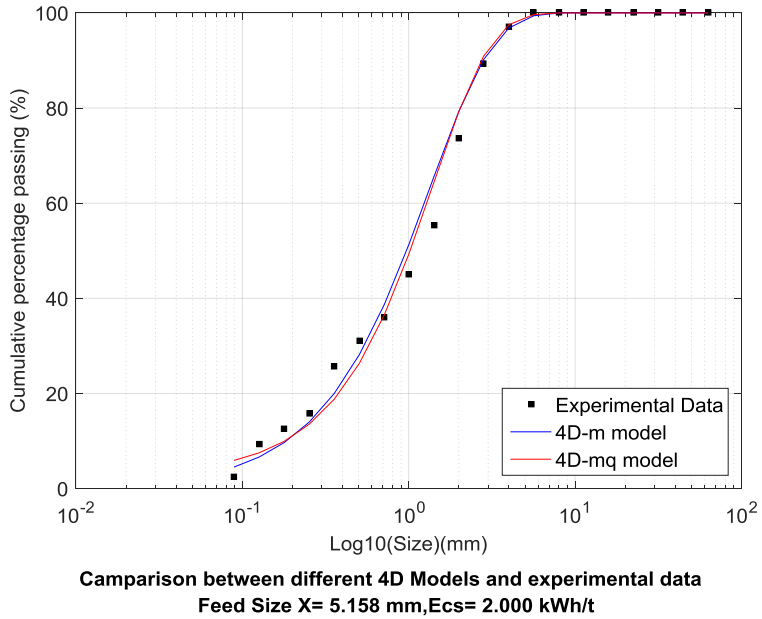

Figure 26 Size distribution comparison (X=5.158 mm, Ecs=2.0 kWh/t)

7. Conclusions

In this work, two versions of the 4D appearance function model, 4D-m and 4D-mq, were developed based on a wide range of breakage test data of mini JKDWT and standard JKDWT. The 4D appearance function models can successfully characterise the breakage of different size-energy combinations (feed size from 425 μm to 63 mm and input specific energy Ecs from 0.1 kWh/t to 2.5 kWh/t). The standard errors (SE) of 4D models are 3.5% and 3.9%, which are more accurate than the JK t_{10}, JK Mpq and King's t_{10} models. Because of the limitation of the functional form of the 4D-m model, it underestimates the cumulative percentage passing at smaller sieve sizes (e.g. sieve size x < 0.212 mm) by about 2%. When the feed size X decreases and the specific energy Ecs decreases, the product size distribution curve becomes steeper, and the underestimation becomes more prominent. The proposed 4D-mq model satisfactorily narrows this gap without undermining the prediction accuracy in other ranges. Overall, the 4D-mq model has the best prediction accuracy.

Compared with the 4D appearance function model developed based on the JKRBT breakage test data (Yu et al., 2016), the 4D appearance function models here (the 4D-m model and the 4D-mq model) have different functional forms and different parameters. However, both of them are based on the P80-m R-R relationship. Considering the 4D models in this work were developed from a wider range of combinations of feed ore sizes and input specific energy, the 4D-m and 4D-mq models in this work have a wider applicable range. The modelling methodology in this work can be applied to other ores to develop a set of ore-specific characterisation parameters, test its wider applicability, and establish a viable appearance function model over wide size and energy ranges.

Acknowledgements

The authors wish to acknowledge the financial support of the Commonwealth Scholarship from the Australian Government and Scholarships from the University of Queensland. The authors wish to acknowledge the partial financial support on supervision from AMIRA P9P project. The reviews and advice on this paper by Dr Marko Hilden and Dr Grant Ballantyne are highly appreciated.

References

Ballantyne, G.R., Powell, M.S., Benchmarking comminution energy consumption for the processing of copper and gold ores. Minerals Engineering, 2014, **65**, 109-114.

Bond, F.C., Crushing tests by pressure and impact. Trans AIME, Am. Inst. Min. Metall. Petrol. Eng. , 1947, **169**, 58-66.

Bourgeois, F.S., Banini, G.A., A portable load cell for in-situ ore impact breakage testing. International Journal of Mineral Processing, 2002, **65(1)**, 31-54.

Evertsson, C.M., 1999. Size reduction in cone crushers, In *Minerals Engineering Conference'99* Falmouth, England.

Evertsson, C.M., 2000. Cone Crusher Performance, In *Department of Machine and Vehicle Design*. Chalmers University of Technology, Göteborg, Sweden.

King, R.P., *Modeling and Simulation of Mineral Processing Systems*. 2nd edn. 2012, Society for Mining, Metallurgy, and Exploration, Inc. (SME), Colorado, US.

King, R.P., Bourgeois, F., Measurement of fracture energy during single-particle fracture. Minerals Engineering, 1993, **6(4)**, 353-367.

Kojovic, T., Hilden, M.M., Powell, M.S., Bailey, C., 2012. Updated Julius Kruttschnitt semi-autogenous grinding mill model In *11th AusIMM Mill Operators' Conference 2012* ed. Hills, P. AusIMM: Australasian Institute of Mining and Metallurgy Hobart, Victoria pp. 71-79.

Leung, K., 1987. An energy based, ore specific model for autogenous and semi-autogenous grinding mills, In *JKMRC*. PhD thesis submitted to the University of Queensland, Brisbane, Australia.

Man, Y.T., 2000. A model-based scale-up procedure for wet overflow ball mills, In *JKMRC, SMI*. PhD thesis submitted to the University of Queensland, Brisbane, QLD, Australia.

Morrell, S., Predicting the specific energy of autogenous and semi-autogenous mills from small diameter drill core samples. Minerals Engineering, 2004, **17(3)**, 447-451.

Napier-Munn, T.J., *Statistical Methods for Mineral Engineers - How to Design Experiments and Analyse Data*. 2014, Julius Kruttschnitt Mineral Research Centre, Sustainable Minerals Institute, The University of Queensland, Australia, Brisbane, QLD 4068, Australia.

Napier-Munn, T.J., Morrell, S., Morrison, R.D., Kojovic, T., 1996. Mineral comminution circuits : their operation and optimisation, First edition 1996, reprinted with minor corrections 1999, 2005 ed. Julius Kruttschnitt Mineral Research Centre, the University of Queensland, Indooroopilly, Brisbane, Australia.

Narayanan, S.S., 1985. Development of a laboratory single particle breakage technique and its application to ball mill modelling and scale-up, In *JKMRC, School of Engineering* PhD thesis submitted to the University of Queensland, Brisbane, Australia, p. 466.

Narayanan, S.S., Whiten, W.J., Determination of comminution characteristics from single particle breakage tests and its application to ball mill scale-up. Trans. Inst. Miner. Metall., 1988, **97**, C115-C124.

Shi, F., A review of the applications of the JK size-dependent breakage model: Part 1: Ore and coal breakage characterisation. International Journal of Mineral Processing, 2016, **155**, 118-129.

Shi, F., Kojovic, T., Validation of a model for impact breakage incorporating particle size effect. International Journal of Mineral Processing, 2007, **82(3)**, 156-163.

Shi, F., Kojovic, T., Brennan, M., Modelling of vertical spindle mills. Part 1: Sub-models for comminution and classification. Fuel, 2015, **143**, 595-601.

Shi, F., Kojovic, T., Larbi-Bram, S., Manlapig, E., Development of a rapid particle breakage characterisation device – The JKRBT. Minerals Engineering, 2009, **22(7–8)**, 602-612.

Shi, F., Xie, W., A specific energy-based ball mill model: From batch grinding to continuous operation. Minerals Engineering, 2016, **86**, 66-74.

Tavares, L.M., 2007. Chapter 1 Breakage of Single Particles: Quasi-Static, In *Handbook of Powder Technology*, eds. Agba D. Salman, M.G., Michael, J.H. Elsevier Science B.V., pp. 3-68.

Tavares, L.M., King, R.P., Measurement of the load–deformation response from impact breakage of particles. International Journal of Mineral Processing, 2004, **74, Supplement**, S267-S277.

Weichert, R., Herbst, J., 1986. An ultra fast load cell for measuring particle breakage, In *World Congress Particle Technology: Part II. Comminution*, pp. 3-15.

Wills, B.A., Napier-Munn, T.J., *Wills' Mineral Processing Technology: an introduction to the practical aspects of ore treatment and mineral recovery*. Seventh edn. 2006, Elsevier, Great Britain.

Yu, P., Xie, W., Liu, L., Powell, M., 2014. Development of a dynamic mill model structure for tumbling mills. , In *XXVII International Mineral Processing Congress - IMPC 2014 Conference Proceedings*, ed. Yianatos, J. Gecamin Digital Publications Santiago, Chile, pp. 41-51.

Yu, P., Xie, W., Liu, L.X., Weerasekara, N., Bonfils, B., Powell, M., 2016. A generic dynamic model incorporating a 4D appearance function for tumbling mills, In *XXVIII International Mineral Processing Congress - IMPC 2016 Conference Proceedings*, Québec City, Canada.